Hydrogen effect on dislocation nucleation in a ferritic alloy Fe-15Cr as observed per nanoindentation

Gaspard Vincent, Guillaume Kermouche, David Delafosse, Afrooz Barnoush

Hydrogen effect on dislocation nucleation in a ferritic alloy Fe–15Cr as observed per nanoindentation

V. Gaspard [a], G. Kermouche [a,*], D. Delafosse [a], A. Barnoush [b]

[a] Ecole Nationale Supérieure des Mines de Saint-Etienne, LGF UMR5307 CNRS, Saint-Etienne, France
[b] Norwegian University of Science and Technology, Department of Engineering Design and Materials, Trondheim, Norway

Hydrogen effects on dislocation nucleation in polycrystalline ferritic Fe–15Cr binary alloy were investigated using in situ electrochemical nanoindentation. Linear elastic finite element calculations taking account of the cubic symmetry of BCC crystals were made to extract the resolved shear stresses on the different slip systems of the indented grains. It is shown that the resolved shear stresses corresponding to the experimentally measured pop-in loads are compatible with homogeneous dislocation nucleation. The resolved shear stress necessary to nucleate dislocations from defect-free crystals was estimated at μ/12–μ/13 without hydrogen. Cathodically charged hydrogen reduces the shear strength of the crystal by 8.5%–19.8%, thus promoting dislocation multiplication.

1. Introduction

Despite intensive investigations through the past decades, the hydrogen effects in iron and its alloys are still controversial. Firstly, the macroscopic effects seem to be very sensitive to experimental conditions, especially to the hydrogen charging conditions. In fact, both hardening [1–3] and softening [4–7] are reported in case of cathodically hydrogen charged pure α-iron whereas no effects on the rheology are visible in cases of any ferritic steels after gaseous hydrogenation [8,9]. Numerous authors noticed that the behavior of hydrogenated iron during conventional mechanical testing depends on the level of purity and on the temperature [10,11] of the material. Moreover, the mechanisms governing those phenomena remain unclear. It is now well established that the flow stress in α-iron, and more generally in BCC materials, is controlled by the mobility of screw dislocations between 0 K and 300 K [12–16]. In this range of temperature, screw segments are subjected to high lattice friction, overcome by a thermally activated mechanism, namely the double kink nucleation. Being given the prevalence of the latter mechanism in the plasticity of α-iron, several attempts were made to attribute the macroscopic hydrogen hardening and softening to interactions between hydrogen atoms and double kink nucleation and propagation [5,17–19]. However, Dong [6] did not obtain distinguishable hydrogen effects on the thermal part of the flow stress, and attributed the observed softening to a decrease of the internal stress, that is to say, to a shielding of the elastic interactions.

The above-mentioned studies are mainly dedicated to hydrogen effects on dislocations mobility. However, the plastic flow of crystalline materials is described by Orowan's law Eq. (1), regardless of the crystal structure:

$$\dot{\varepsilon} = \rho b v \tag{1}$$

where $\dot{\varepsilon}$ is the strain rate, ρ the mobile dislocation density, b the Burger vector and v the dislocations velocity. In the frame of the present work, we focus on the hydrogen effects of the dislocation density in ferritic alloys. In other words, this study aims to investigate the hydrogen effects on dislocations multiplication. In case of b.c.c. metals, the multiplication phase occurs during the very first stage of plastic strain and consists in creating screw segments by edge segments dragging from initial dislocation configuration [20,21].

It has been demonstrated that the nanoindentation technique provides an efficient way of characterizing the stress required for dislocation nucleation. In particular, if the indented volume is considered as free from defects, the pop-in, which is a sudden increase of the displacement of the tip at a constant load, is shown to be the consequence of a homogeneous dislocation nucleation (HDN) [22,23]. Nanoindentation has already been used to investigate the hydrogen effects in crystalline materials [24]. In particular,

* Corresponding author. Tel.: +33 477 420 074.
E-mail address: kermouche@emse.fr (G. Kermouche).

the in situ electrochemical nanoindentation has been recently developed and successfully applied to investigate the hydrogen effect on dislocation nucleation and on dislocation mobilities in different metals and alloys [25–30]. The purpose of this work is to examine the hydrogen effect on dislocation nucleation in the high purity ferritic binary alloy Fe–15Cr.

2. Experimental

The material used in this study is a polycrystalline ferritic binary alloy Fe–15Cr produced by zone melting. The chemical composition is given in Table 1. Swaged cylindrical rods, 14 mm in diameter, were annealed at 700 °C during 2 h. A disc of thickness 3 mm was cut and heat treated in vacuum at 650 °C during 48 h to finally obtain a mean grain size of about 500 μm and a low dislocation density. The specimen was mechanically polished up to 0.25 μm. An Electron Back Scattering Diffraction (EBSD) mapping of the sample revealed the crystallographic orientations of each grain at the surface (Fig. 1). Three grains with different crystallographic orientations, denominated grain A, grain B, and grain C in the following, are chosen to undergo nanoindentation tests. Their exact crystallographic orientations defined by Euler angles (φ_1, Φ, φ_2) [31] are given in Table 2. The Euler angles are related to the crystal orientation in the coordinate system defined with the normal to the sample surface, also corresponding to the indentation direction. Just before nanomechanical testing, the specimen was electropolished in a 1 M H_2SO_4 methanolic solution at 20 V for 30 s. The surface roughness was controlled with an atomic force microscope (AFM) and evaluated with a root mean square (RMS) of about 1 nm on 1 μm^2.

The experiments were carried out with a Hysitron TI 950 Triboindenter® equipped with a Berkovitch diamond tip. A three electrode setup with a platinum wire as counter electrode and an Hg/Hg_2SO_4 reference electrode was used. In the following, all the electrochemical potentials will be reported against this reference electrode. An electrochemical cell made of Teflon® and containing

Table 1
Chemical composition of Fe–15Cr.

Elements	Fe	Cr	C	O	N	S
Concentration	–	14.90 wt%	21 wt ppm	4 wt ppm	2 wt ppm	2 wt ppm

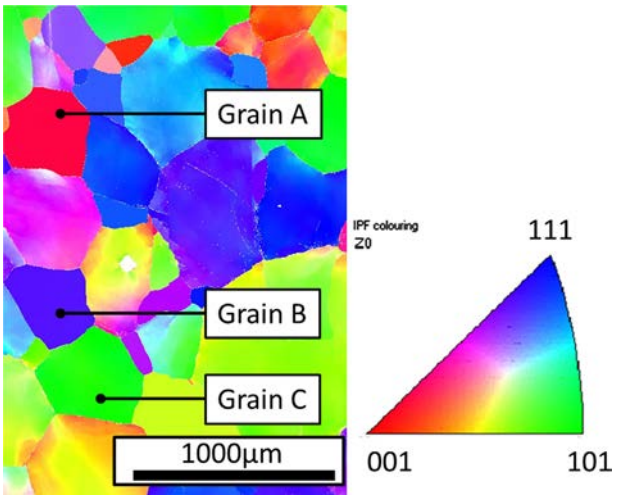

Fig. 1. Inverse Pole Figure obtained by EBSD mapping of the sample's surface.

Table 2
Crystallographic orientations of the indented grains.

	φ_1 (deg)	Φ (deg)	φ_2 (deg)
Grain A	100	10.7	46.7
Grain B	288	41.5	42.5
Grain C	88	40	89

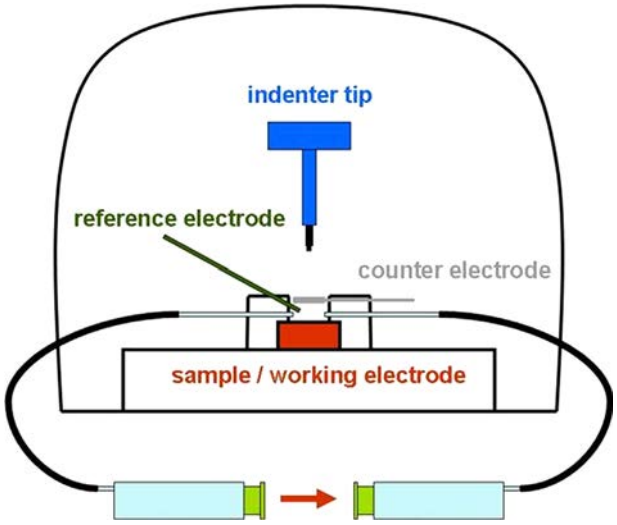

Fig. 2. Experimental setup.

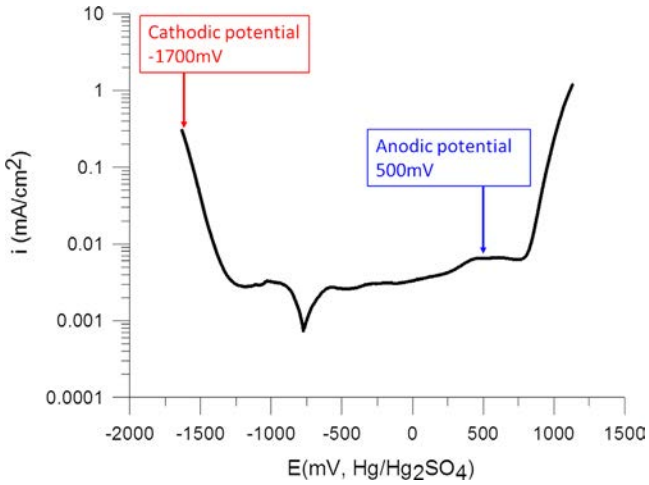

Fig. 3. Polarization curve of Fe–15Cr in 0.05 M Na_2SO_4 with a sweeping rate of 10 mV/s.

the sample was filled with approximately 0.23 mL of electrolyte for hydrogen charging. The electrolyte was a 0.05 M Na_2SO_4 solution with a pH equal to 5.93. The experimental setup is schematically shown in Fig. 2. Series of 25 indentations under cathodic potential and of 50 indentations under anodic potential were alternately performed on each grain. In agreement with the previously established polarization curve (Fig. 3) of the specimen in the same electrolyte, the cathodic and anodic potentials were set to −1700 mV and 500 mV, respectively. The loading was performed with an 8000 μN/s loading rate up to 2000 μN followed with a holding time of 0.5 s at this maximum load. An additional 0.25 s holding time at 10% of the peak load was used for drift correction, as shown in Fig. 4. The indents are made far enough

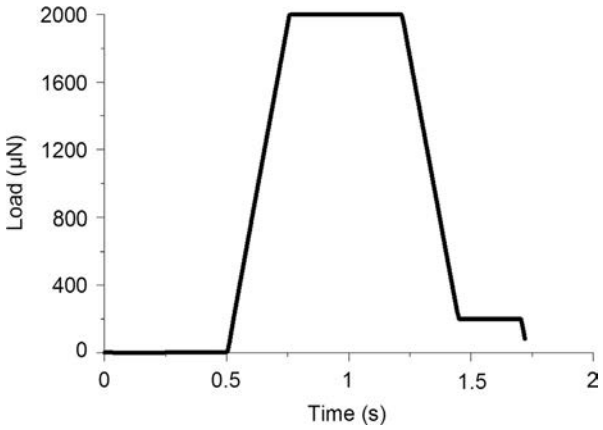

Fig. 4. Load function used for nanoindentations.

from the grain boundaries, so that they do not influence the response of the crystal to nanoindentation.

3. Results

3.1. Pop-in loads

Typical load–displacement curves under cathodic and anodic polarization are given in Fig. 5. They correspond to indentations made in grain B. Similar reductions of the pop-in loads are obtained in grains A and C. The response of the material during the loading part of the indentation test can be described in three stages. After a first elastic loading, a discontinuous displacement step appears at the onset of plasticity at constant load. This excursion in depth is named pop-in and is characterized by a pop-in load and a pop-in width. A pop-in was observed for every indent. The last part of the loading curve corresponds to the continuous elasto-plastic deformation. It may be seen from Fig. 5 that the pop-in occurs for deformations higher than 15 nm. Consequently, any effects of oxide layer on the pop-in can be ruled out since thicknesses of native oxides layers do not exceed 4 nm in iron chromium alloys at room temperature when exposed to acid solutions [32]. In particular, Sugimoto and Sawada [33] showed with ellipsometry that Fe (5–60)Cr alloys do not produce oxide thicknesses higher than 3.2 nm in a 1 M Na_2SO_4 solution. Pop-in loads distributions in the three indented grains under anodic and cathodic polarizations are presented in Fig. 6. It can be seen from Fig. 6 that the pop-in loads strongly depend on the crystallographic orientations of the grains, regardless of the polarization. It is clearly shown that pop-in loads are lower under cathodic polarization than under anodic polarization. This phenomenon is reproducible and appears in the three grains. The mean pop-in loads obtained in grains A, B and C under anodic and cathodic polarization are given in Table 3.

3.2. Resolved shear stress

In case of annealed materials, the dislocation density can range between $10^6/cm^2$ and $10^8/cm^2$ [34,35]. This corresponds to spacings of 1–10 μm [28] between dislocations, whereas considering the Hertzian contact model, the loaded region during nanoindentation is confined within a radius of 200 nm at the pop-in [28]. Consequently, at the scale of the experiments, the crystal lattice is considered to be defect-free prior to indentation. Homogeneous dislocation nucleation occurs when the critical shear stress of the crystal is reached under the tip of the indenter. The shear stress required to emit a dislocation from a perfect lattice is defined on

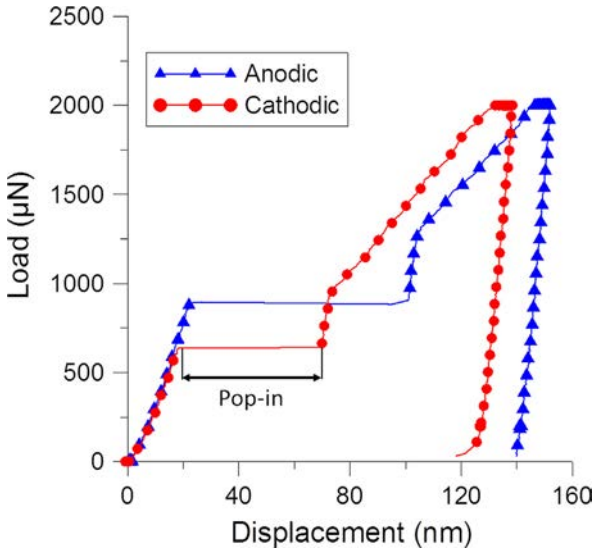

Fig. 5. Typical load–displacement curves under anodic and cathodic polarization corresponding to grain B.

the slip systems and is therefore named Critical Resolved Shear Stress (CRSS). Slip occurs on the most favorably oriented slip system with regard to the loading direction, in other words on the slip system having the highest Schmid factor. The maximal shear stress τ_{max} beneath the indenter tip and the corresponding depth $z_{\tau_{max}}$ can be evaluated using the continuum mechanics theory [36]:

$$\tau_{max} = 0.31\left(\frac{6E_r^2}{\pi^3 R^2}\right)^{1/3} \tag{2}$$

$$z_{\tau_{max}} = 0.48\left(\frac{3PR}{4E_r}\right)^{1/3} \tag{3}$$

where P is the applied load, R the radius of the Berkovitch tip and E_r the reduced modulus given by

$$\frac{1}{E_r} = \frac{1-\nu_1^2}{E_1} + \frac{1-\nu_2^2}{E_2} \tag{4}$$

where subscript 1 corresponds to the diamond tip and subscript 2 to the indented material. E and ν are Young's moduli and Poisson's ratios of the solids. The tip radius can be estimated by fitting the Hertzian contact mechanics model (Eq. (5)) to the elastic part of experimental load–displacement curves [36].

$$P = \frac{4}{3}E_r\sqrt{R}h^{3/2} \tag{5}$$

where h is the indenter penetration depth.

The maximal shear stress obtained using the simple approach of the linear isotropic elasticity presented above does not have a particular significance if the material is considered as an oriented anisotropic crystal in which slip occurs in specified planes and directions. If it provides a widely used approximation of the absolute value of the maximal shear stress under the tip during indentation [28,30], the described method cannot explain the observed crystallographic orientation dependence of the mean pop-in loads shown in Table 3. In order to evaluate the shear stresses resolved in the slip systems, induced by the indentation, and corresponding to the pop-in loads in the three indented grains, a linear cubic elastic Finite Element Model (FEM) was developed using Abaqus®. The radius of the tip used in the FE calculations is evaluated by fitting Hertzian's contact model to the elastic part of the experimental curves and is found to be equal to R=750 nm. Due to the lack of available data, the three elastic constants corresponding to the cubic symmetry have been chosen

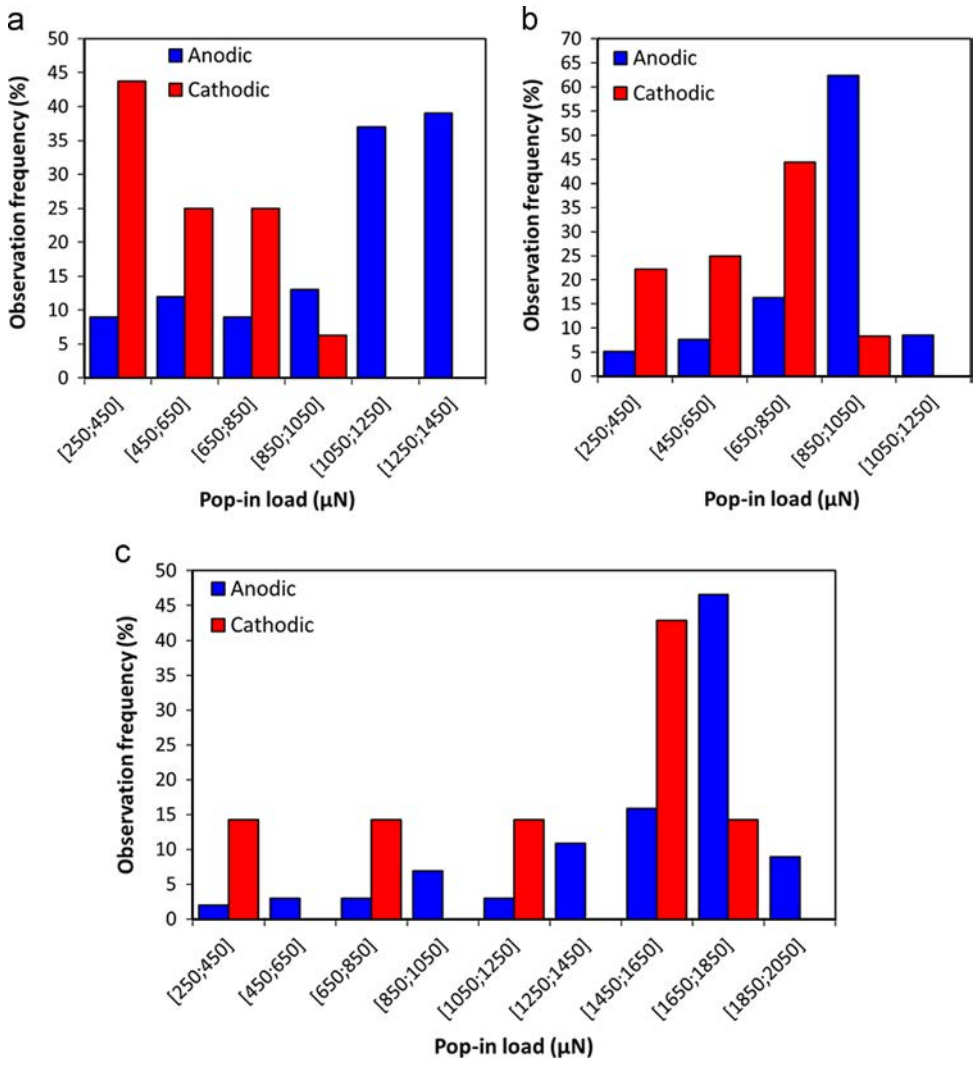

Fig. 6. (a) Pop-in load distribution under anodic and cathodic polarization in grain A, (b) grain B, (c) grain C.

Table 3
Mean pop-in loads under different polarizations.

Mean $P_{pop\text{-}in}$ (μN)	Grain A	Grain B	Grain C
Anodic	1048	882	1527
Cathodic	558	627	1150

to be those of pure iron – $C_{11}=237$ GPa, $C_{12}=141$ GPa and $C_{44}=116$ GPa [37]. The elastic properties of the tip are those of diamond ($\nu=0.07$ and $E=1140$ GPa [26]). The orientations of the crystals with regard to the applied load direction are given by Euler's angle in Table 2. The resolved shear stresses are calculated for grains A, B and C, in the 12 slip systems of the b.c.c. lattices corresponding to the dense planes {110} and the dense directions ⟨111⟩. For each grain, the slip system presenting the highest shear stress is identified, and the load versus the resolved shear stress on this slip system of the highest Schmid factor is plotted in Fig. 7. The maximal shear stress calculated as per Eq. (2) and corresponding to the analytical solution given by the Hertzian contact theory is plotted as a reference. It clearly appears that the Hertzian analytical solution is an upper bound of the resolved shear stresses in the crystal. The discrepancies between the analytical solution and the resolved shear stresses obtained with FEM simulations

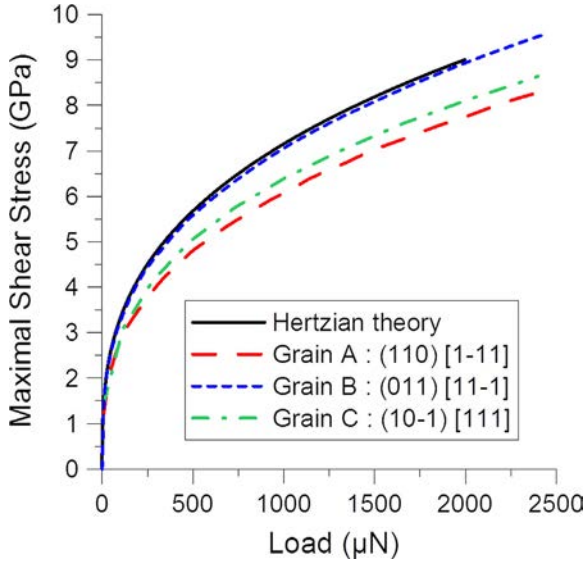

Fig. 7. Resolved shear stresses versus applied load in grains A, B and C and maximal shear stress calculated with the Hertzian contact based isotropic model. The corresponding slip systems of the highest Schmid factor for the three grains are given in the legend.

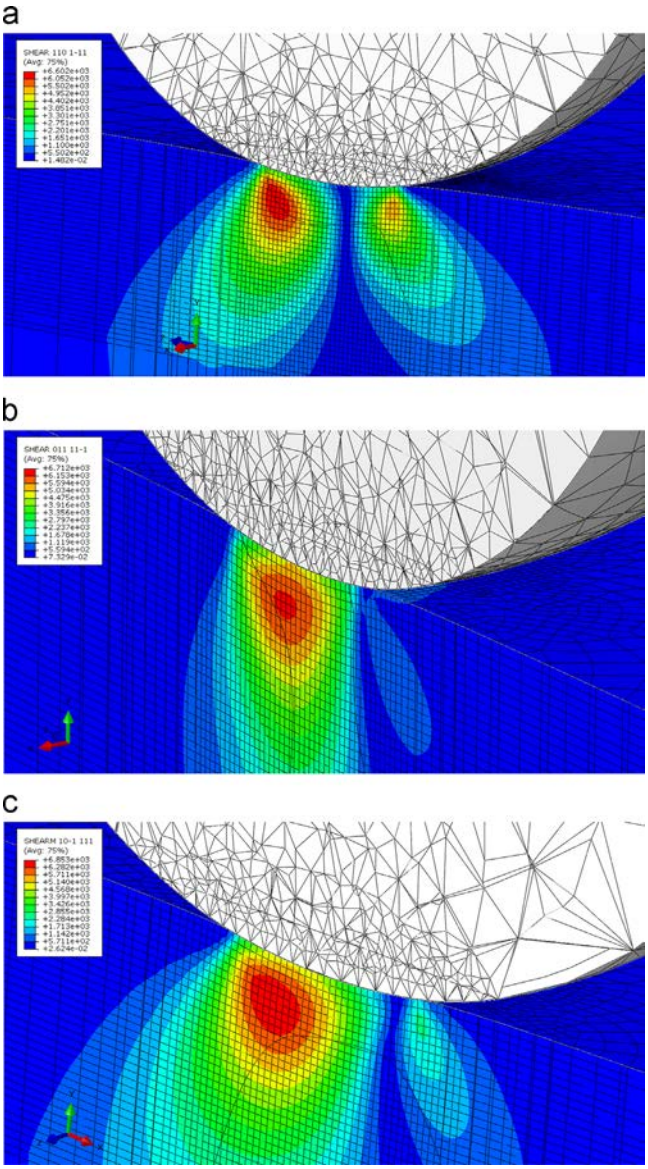

Fig. 8. (a) Resolved shear stress distribution in the slip system (110)[1 – 11] under the indenter in grain A. Stresses are given in MPa. (b) Resolved shear stress distribution in the slip system (011)[11 – 1] under the indenter in grain B. Stresses are given in MPa. (c) Resolved shear stress distribution in the slip system (10 – 1)[111] under the indenter in grain C. Stresses are given in MPa.

Table 4
Resolved shear stresses corresponding to the pop-in loads in grains A, B and C under different polarizations.

		Slip system	$\tau_{pop\text{-}in}$ (GPa)	$\tau_{pop\text{-}in}/\mu$
Grain A	Anodic	(110)[1–11]	6.21	1/13
	Cathodic		4.98	1/17
Grain B	Anodic	(011)[11 – 1]	6.75	1/12
	Cathodic		5.98	1/14
Grain C	Anodic	(10 – 1)[111]	7.10	1/12
	Cathodic		6.50	1/13

correspond to differences in the position of the maximal shear stress under the tip [23,38]. Fig. 8 puts in evidence the considered slip system dependence of the position of the maximal resolved shear stress beneath the indenter. The load versus resolved shear stress curves allow evaluating the resolved shear stress corresponding to the mean pop-in load value on the slip system with the highest Schmid factor. The resolved shear stresses, $\tau_{pop\text{-}in}$, corresponding to the mean pop-in loads in grains A, B and C under anodic and cathodic polarizations are given in Table 4. Since the shear modulus of α-iron single crystals, μ, is approximately equal to 83 GPa [39], shear stresses can be presented as ratios. Under anodic polarization, $\tau_{pop\text{-}in}$ is approximately in the range μ/12–μ/13, whereas under cathodic polarization, it ranges between μ/13 and μ/17. Cathodic polarization induces a decrease of the resolved shear stresses calculated on the slip systems having the highest Schmid factors of 19.8%, 11.5% and 8.5% in grains A, B and C, respectively.

4. Discussion

The experimentally observed decrease of the pop-in load with the increase in hydrogen concentration is consistent with the results of different authors. This phenomenon, in conjunction with a decrease of the pop-in width, has been shown to appear in different materials like vanadium [30], nickel [27], and Fe–3%Si [29]. Assumption is made that the pop-in phenomenon is a manifest of HDN, as it cannot be due to the rupture of oxide layers and as the probability of activating an existing dislocation source is very low. From this point of view, shear stresses must be resolved in the activated slip system to be significant at this scale. A linear orthotropic elastic finite element analysis was conducted to estimate the resolved shear stresses corresponding to pop-in loads in every slip system, whatever the orientation of the grain. It has been demonstrated that the isotropic analytical calculation, based on the Hertzian contact theory, is in good agreement with the FEM calculations, even if it does not discriminate the different slip systems. Considering that the slip systems are of the ⟨111⟩{110} type [16], and that a unique slip system is activated during the pop-in, this one being the slip system of the highest Schmid factor, it should be shown that $\tau_{pop\text{-}in}$ corresponds to the theoretical shear strength of the material.

In fact, without the influence of hydrogen, under anodic polarization, the calculated $\tau_{pop\text{-}in}$ is in the range μ/12–μ/13 whereas the theoretical shear strength of the crystalline metals is generally considered to be $\mu/2\pi$–μ/30 [26,40]. Moreover, $\tau_{pop\text{-}in}$ does not vary too much with the crystal orientation. In other words, $\tau_{pop\text{-}in}$ remains unchanged from grain to grain, i.e. is equal in the different activated slip systems operating in grains A, B and C. This is fairly coherent with HDN and thereby supports the above initial assumption. In addition, detailed studies of local plasticity in MgO [41,42] showed that pre-existing dislocations lead to a decrease of the observed pop-in load. If the initial dislocation density in the present study is low, its influence cannot be completely ruled out. In particular, it could explain the scattering of the observed pop-in load distributions presented in Fig. 6.

Furthermore, the coherence of the latter results states the efficiency of such FE analysis in determining with a sufficient precision the resolved shear stresses in a crystal during elastic loading. The benefit of using such methods is a higher precision than using the isotropic model in estimating the maximal shear stress beneath the indenter. For instance, at an applied load of 1000 μN, the isotropic model based on the Hertzian contact theory overestimates by 19% the maximal shear stress in grain A. However, the experimentally obtained mean pop-in load is higher in grain C than in grain A, and a higher calculated maximal shear stress in grain A than in grain C would be expected. This is not the result given by the FEM simulations, but this can be explained by the large value of the mean misorientation angle in the grain C (6.9°), indicating that the crystallographic orientation is less

homogeneous in this grain than in the two other grains (mean misorientation angle of 0.4° in grains A and B).

The above-presented results lead to the conclusion that hydrogen, introduced in the material by cathodic polarization, promotes HDN. The reduction of the resolved pop-in shear stress due to hydrogen ranges between 8.5% and 19.8%. This can be explained by the defactant concept first introduced by Kirchheim [43] and then applied to hydrogen effects in nanoindentation tests [29]. According to this theory, the hydrogen induced decrease of the HDN activation energy is the consequence of a reduction of the stacking fault energy and of a decrease of the interatomic bonding energy, that is to say a reduction of the cohesion of the crystal lattice. This is in good agreement with the lowering of the shear modulus obtained by Lunarska et al. in pure iron [44] and with the molecular static simulation of Taketomi et al. [45].

The hereby reported hydrogen enhanced nucleation of dislocations is compatible with an increase of the mobile dislocation density, and thus with a softening of the material. This is in good agreement with the transmission electron micrographs of Matsui et al. [1] showing that cathodically charged hydrogen increases the dislocation density in case of pure iron deformed at 3.0% at 200 K by conventional tensile testing. Tabata and Birnbaum [18] also reported an increase of the dislocation density in pure iron when exposed to gaseous hydrogen using in situ deformation technique in an electron microscope. If the enhancement of dislocation multiplication with hydrogen contributes to a softening in the early stages of the deformation, it is believed that it could also harden the specimen in the later stages of the deformation, as the density of forest dislocations may increase [18,46]. In particular, this corresponds to the experimental results of Matsui et al. [4] obtained by tensile testing of cathodically pre-charged pure iron specimen. The present work shows that in the case of the ferritic alloy Fe–15Cr and in the described experimental conditions, the hydrogen effects on dislocation multiplication during conventional mechanical testing may be due not only to the activation of pre-existing Frank-Read sources, but also to the dislocation nucleation from defect-free volumes (HDN).

5. Conclusion

The effect of hydrogen on dislocation nucleation in the ferritic alloy Fe–15Cr has been identified by in situ electrochemical nanoindentation testing. It has been demonstrated that the pop-in load is decreased in the presence of hydrogen. Moreover, this study put in evidence that linear elastic finite element analysis provides an efficient way of taking into account the crystal anisotropy and of calculating the resolved shear stresses in a given slip system. Although the results from FEA globally well agree with results from isotropic calculations using the Hertzian contact theory, FEA allows a higher precision on estimating the maximal shear stress value and its position under the indenter. In particular, the discrepancy between the two methods depends on the considered slip system, and consequently, on the orientation of the crystal. The evaluation of the resolved stresses corresponding to the pop-in loads showed that pop-in occurs due to HDN in this material. The theoretical shear strength in Fe–15Cr has been quoted at $\mu/12$–$\mu/13$ without the influence of hydrogen and a decrease of 8.5%–19.8% was found under cathodic polarization. The highlighted hydrogen effect is a decrease of the critical resolved shear stress promoting HDN and consequently increasing the dislocation density. This phenomenon is believed to be one of the origins of hydrogen softening observed in the first stages of plastic strain during conventional mechanical testing.

References

[1] H. Matsui, H. Kimura, S. Moriya, Mater. Sci. Eng. 40 (1979) 207–216.
[2] S. Asano, R. Otsuka, Scr. Metall. 10 (1976) 1015–1020.
[3] S. Asano, R. Otsuka, Scr. Metall. 12 (1978) 287–288.
[4] S. Moriya, H. Matsui, H. Kimura, Mater. Sci. Eng. 40 (1979) 217–225.
[5] H. Matsui, H. Kimura, A. Kimura, Mater. Sci. Eng. 40 (1979) 227–234.
[6] H. Dong, A.W. Thompson, Mater. Sci. Eng. A 188 (1994) 43–49.
[7] E. Lunarska, V. Novak, N. Zarubova, S. Kadeckova, Scr. Metall. 17 (1983) 705–710.
[8] I. Moro, L. Briottet, P. Lemoine, E. Andrieu, C. Blanc, G. Odemer, Mater. Sci. Eng. A 527 (2010) 7252–7260.
[9] T. Michler, J. Naumann, Int. J. Hydrogen Energy 35 (2010) 821–832.
[10] K. Oguri, H. Kimura, Scr. Metall. 14 (1980) 1017–1022.
[11] A. Zielinski, E. Lunarska, M. Smialowski, Acta Metall. 25 (1977) 551–556.
[12] M.S. Duesbery, Philos. Mag. 19 (1969) 501–526.
[13] M. Tang, L.P. Kubin, G.R. Canova, Acta Mater. 46 (1998) 3221–3235.
[14] M. Tang, M. Fivel, L. Kubin, Mater. Sci. Eng. A 309–310 (2001) 256–260.
[15] W. Spitzig, Acta Metall. 18 (1970) 1275–1284.
[16] D. Caillard, Acta Mater. 58 (2010) 3493–3503.
[17] S. Wang, N. Hashimoto, S. Ohnuki, Mater. Sci. Eng. A 562 (2013) 101–108.
[18] T. Tabata, H.K. Birnbaum, Scr. Metall. 17 (1983) 947–950.
[19] M. Wen, S. Fukuyama, K. Yokogawa, Acta Mater. 51 (2003) 1767–1773.
[20] N. Brown, R. Ekvall, Acta Metall. 10 (1962) 1101–1107.
[21] H. Solomon, G. McMahon, Acta Metall. 19 (1971) 291–302.
[22] D. Catoor, Y.F. Gao, J. Geng, M.J.N.V. Prasad, E.G. Herbert, K.S. Kumar, G. M. Pharr, E.P. George, Acta Mater. 61 (2013) 2953–2965.
[23] T.L. Li, Y.F. Gao, H. Bei, E.P. George, J. Mech. Phys. Solids 59 (2011) 1147–1162.
[24] Y. Katz, N. Tymiak, W.W. Gerberich, Eng. Fract. Mech. 68 (2001) 619–646.
[25] A. Barnoush, M. Asgari, R. Johnsen, Scr. Mater. 66 (2012) 414–417.
[26] A. Barnoush, Acta Mater. 60 (2012) 1268–1277.
[27] A. Barnoush, H. Vehoff, Scr. Mater. 55 (2006) 195–198.
[28] A. Barnoush, H. Vehoff, Corros. Sci. 50 (2008) 259–267.
[29] A. Barnoush, H. Vehoff, Acta Mater. 58 (2010) 5274–5285.
[30] E. Tal-Gutelmacher, R. Gemma, C.A. Volkert, R. Kirchheim, Scr. Mater. 63 (2010) 1032–1035.
[31] H.-J. Bunje, Texture Analysis in Materials Science: Mathematical Methods, first ed., Butterworth-Heinemann, Boston, 1983.
[32] S. Jin, A. Atrens, Appl. Phys. A Solids Surf. 50 (1990) 287–300.
[33] K. Sugimoto, Y. Sawada, Corros. Sci. 17 (1977) 425–445.
[34] C. Dunn, E. Kogh, Acta Metall. 5 (1957) 548–554.
[35] D. Moon, Mater. Sci. Eng. 7 (1971) 103–108.
[36] K.L. Johnson, Contact Mechanics, ninth ed., Cambridge University Press, Cambridge, 2003.
[37] H.M. Ledbetter, R.P. Reed, J. Phys. Chem. Ref. Data 2 (1973) 531–662.
[38] I. Salehinia, S.K. Lawrence, D.F. Bahr, Acta Mater. 61 (2013) 1421–1431.
[39] G. Ghosh, G.B. Olson, Acta Mater. 50 (2002) 2655–2675.
[40] J. Friedel, Dislocations, first ed., Pergamon Press Ltd., Reading, 1964.
[41] Y. Gaillard, C. Tromas, J. Woirgard, Acta Mater. 54 (2006) 1409–1417.
[42] A. Montagne, V. Audurier, C. Tromas, Acta Mater. 61 (2013) 4778–4786.
[43] R. Kirchheim, Int. J. Mater. Res. (formerly Z. Metall.) 100 (2009) 483–487.
[44] E. Lunarska, A. Zielinski, M. Smialowski, Acta Metall. 25 (1977) 305–308.
[45] S. Taketomi, R. Matsumoto, N. Miyazaki, Int. J. Mech. Sci. 52 (2010) 334–338.
[46] M. Deutges, I. Knorr, C. Borchers, C.A. Volkert, R. Kirchheim, Scr. Mater. 68 (2013) 71–74.